Nonlinear piezoelectric properties of epitaxial $BaTiO_3$ thin film

B. Negulescu[1 a], C. J. M. Daumont[1], J. Sakai[1], A. Ruyter[1],
M. Bavencoffe[2], N. Alyabyeva[3] and J. Wolfman[1]

1. GREMAN, Univ. F. Rabelais, Tours, 37200, France
2. GREMAN, INSA Centre Val de Loire, Blois, 41034, France
3. ISMO, Univ. Paris-Sud, Orsay, F-91405, France

The piezoelectric properties of epitaxial $BaTiO_3$ film were studied by double laser Doppler vibrometry. As expected for a ferroelectric material, the piezoelectric response of the structure is hysteretic. The d_{33} value is reduced from a maximum 42 pm/V to 25 pm/V when increasing the DC bias, indicating the large influence of extrinsic effects close to the coercive fields. Using a Rayleigh approach, the slight nonlinearity of the piezoelectric response as a function of the AC field was attributed to irreversible domain wall displacements. At high AC electric fields the strain saturates. The second harmonic response of the system was associated to the piezoelectric activity.

Introduction

The last decades showed an increased interest in the development of integrated piezoelectric thin films for sensor, actuator and transducer applications [1-3]. From the materials point of view, perovskites oxides are optimal choices as they can show excellent piezoelectric properties. Some of the perovskites oxides are ferroelectric below their Curie temperature and one can distinguish several mechanisms contributing to the piezoelectric character, such as the polarization stretching, the rotation of the polarization vector or the domain wall motion. When the electric field is applied parallel to the polarization vector, the lattice elongates in the direction of the field, so inducing an extension of the polarization. This mechanism can be defined as a material intrinsic piezoelectric effect. The rotation of the polarization vector is usually observed in morphotropic phase boundary systems where two phases with different polarization directions coexist. In these conditions, the energy barrier between the different directions of polarization is reduced and the polarization rotation is favored [4]. Other mechanisms can also induce the rotation of the polarization vector, as the epitaxial strain [5]. The

a) Electronic mail : negulescu@univ-tours.fr

displacement of the ferroelectric domain walls is associated with local shape changes of the crystallographic structure and it is considered as an extrinsic material contribution to the piezoelectricity.

The piezoelectric coefficients measured in thin films are generally much lower than those obtained in bulk materials, mostly for two reasons: one is that the films are clamped by the rigid substrates and the lattice cannot extend as in a free piezoelectric structure [3] and the other is that the mobility of the ferroelastic domain walls is reduced by defects or interfacial pinning [6,7] hence the extrinsic contribution to the piezoelectric effect is smaller than in bulk material.

Here we investigate the piezoelectric properties of epitaxial $BaTiO_3$ (BTO) thin films. BTO is a lead free material showing piezoelectric coefficients of 90 pm/V in the single-crystal forms [8] that can be enhanced up to 500 pm/V in optimized ceramics [9]. BTO thin films were extensively studied mostly from the viewpoint of their dielectric, ferroelectric and electro-optic properties (for some examples see [10-12]) while quite few reports are published on their piezoelectric properties.

Among the various thin film fabrication methods, pulsed laser deposition (PLD) is widely used to prepare epitaxial oxide layers and heterostructures. In this technique the oxygen pressure and the laser fluence strongly influence the film stoichiometry and thus the resulting physical properties [13-18]. In this study the PLD technique was used to deposit epitaxial BTO film with optimal parameters that were extracted from published literature. The piezoelectric properties of this system were studied in order to distinguish between the intrinsic and the extrinsic effects and to identify the influence of each of these two contributions on the nonlinearity of the piezoelectric response.

Experimental

100 nm thick $BaTiO_3$ film was epitaxially deposited on (100) $SrTiO_3$ (STO) single crystalline substrate by PLD technique using a KrF excimer laser working at 248 nm. The laser fluence was set to 1.5 J/cm^2 and the substrate temperature to 700°C. The oxygen pressure was kept at 0.1 Torr during the deposition then increased at 300 Torr for the cool down period. For 2 Hz repetition rate of the laser pulses and a target-sample distance of 5 cm, the deposition rate is 0.7 Å/sec. As bottom electrode, a 34 nm thick $SrRuO_3$ (SRO) film was deposited with the same laser conditions, 625°C substrate temperature and 0.15 Torr O_2 pressure. The growth of the film was monitored in-situ by RHEED. Ni (30nm) covered by Au (10 nm) top electrodes were prepared by lift off technique and e-beam evaporation.

The ferroelectric properties were studied using a Precision LC Radiant tester and I(V) curves measured with an Agilent precision source/measure unit. The piezoelectric characterization was realized with a MSA 500 laser Doppler vibrometer from Polytech using a VD-06 high precision velocity decoder that gives a detection resolution in the pm range. A differential measurement realized with 2 beams, the measuring beam positioned on top of the electrode and the reference beam situated in the vicinity of the top electrode, allow to remove the substrate bending effects [19,20]. The internal generator allows to apply simultaneously an alternative signal and a DC bias with a maximum total value of 10 V. The frequency used for the excitation signal was 15 kHz and the response of the system was measured either at 15 kHz (1st harmonic) or at 30 kHz (2nd harmonic).

Results and discussions

θ – 2θ diffractograms (fig.1a) and mapping of the reciprocal space (fig. 1b) were used to characterize the crystallographic structure of the samples. The θ – 2θ XRD pattern shows only the (00L) reflections originating from the substrate, the SRO electrode and the BTO film. Two peaks are observed for the BTO film. The same contributions are identified in the reciprocal space map (RSM) around the (103) reflection. The lattice parameters calculated from these scans are presented in Table I. The less intense BTO peak has the in plane parameter identical to that of the STO substrate (3.905 Å), therefore it comes from a strained part of the film (BTO – s). The second peak is assigned to a relaxed BTO component (BTO – r) that has lattice parameters close to those of the tetragonal bulk BTO (a = 3.994 Å, c = 4.038 Å). The relative intensity of the BTO peaks suggest that most of the film is in the BTO-r state. These results indicate a tetragonal growth of the BTO film with the c axis oriented perpendicular to the substrate.

Table I: Lattice parameters extracted from the θ – 2θ scan and the RSM.

	a (Å)	c (Å)
STO	3.905	3.905
SRO	3.905	3.949
BTO-s	3.9047	4.149
BTO-r	3.984	4.032

As often reported in the literature [21,22] a change from 2D to 3D growth mode is observed for BTO films onto STO substrates after just a few monolayers, related to the relaxation of the epitaxial strain. This

growth mode is confirmed by the RHEED analysis (see fig. 1c). The 2D streaks observed before the BTO deposition are transformed in spots after a few minutes of deposition and the RHEED intensity oscillates only during the first unit cells. Figure 1d shows the topography of the film for a 3x3 μm^2 surface, obtained by atomic force microscopy (AFM) in tapping mode. The topography measured on the film that have a thickness of about 250 unit cells shows a grainy surface, with small grains of a few tens of nanometers in diameter. The roughness analysis of the surface gives 2.5 nm RMS.

The ferroelectric character of the film was evidenced either by quasistatic P(V) and I(V) measurements or by dynamic piezoelectric measurements (fig.2). In these experiments the bias is applied on the top electrode while the bottom electrode is grounded. A hysteretic behavior is observed in all the measurements, with a shift of the loops towards the negative bias region. This shift is generally related to an internal built-in field due to the screening of the depolarization field and/or ionic/dipole defects in the film [23, 24]. One can notice that the P(V) loop is not only shifted on the field axis but also asymmetrical. This irregular shape can be analyzed as a measurement artefact due to leakage currents. As the LC tester measures the electrical charge, the response of a lossy sample is dependent not only on the polarization PS, but also on the leakage current density J during the measurement [25, 26] :

$$Q/S = 2 \cdot P_S + \int J \cdot dt \qquad (1)$$

As the leakage current is larger in negative voltage than in the positive region (fig 2b), asymmetric polarization loops can be obtained in this kind of measurement. The I(V) curve also confirms the ferroelectric character of the film since peaks in the current, corresponding to ferroelectric switching, can be seen at the coercive fields.

The vibrometer measures the vertical displacement of the top electrode under a certain excitation field. Several harmonics are observed and the piezoelectric d_{33} parameter is obtained by dividing the displacement value, measured for the 1st harmonic, by the amplitude of the AC excitation voltage. Fig. 2c presents the piezoelectric response of the sample measured as a function of the DC bias with an excitation voltage of 0.25 V at 15 kHz. The minimum values of d_{33} are associated with the polarization switching fields. We note that the coercive field obtained from this dynamic measurement, 0.5 MV/m, is much smaller than the value obtained in the quasistatic measurements that gives about 1.5 MV/m. This difference probably comes from the value used for the excitation field (0.25 V $\Leftrightarrow$2.5 MV/m), which is higher than that of the quasistatic coercive field.

The d_{33} value in positive bias decreases slowly with the voltage from a maximum value of 42 pm/V to 26 pm/V at 7V (not shown here). In negative bias the d_{33} value stabilizes at 25 pm/V for voltages below -2V (not

shown here). The maximum d_{33} value measured in our film is comparable to those obtained in equivalent systems but with thicker films: 50 pm/V for 400 nm thick $BaTiO_3$-$CoFe_2O_4$ nanostructured films [27], 62 pm/V for 700 nm thick RF sputtered epitaxial $BaTiO_3$ films [28] and 50 pm/V for 180 nm thick epitaxial $BaTiO_3$ films [29].

The increased value of the piezoelectric coefficient around the switching field can be attributed to extrinsic effects related to the presence of domain walls (DW) in the film. As the sample has a tetragonal structure with the polarization c axis oriented perpendicular to the film surface, only 180° polarization domains are expected in the film. Since 180° DWs are not ferroelastic, they should not contribute to the piezoelectric effect. Nevertheless, 90° DW can still be present in the film as already observed in c-oriented tetragonal PZT films [30] where the mixture of a and c domains is expected to accommodate the epitaxial strain. Several papers [31, 32] argued that 180° DWs participate to the piezoelectric response of a system mainly through two mechanisms: converse piezoelectric effect in the DW under electric field and substrate clamping. The first can be understood as induced strain inside the 180° DWs when some domains are extending while the adjacent ones are contracting. The second mechanism suppose that 180° DW motion can lead to substrate bending contribution that enhances the piezoelectric response of the structure.

In order to distinguish extrinsic effects from intrinsic ones, the sample was driven in different ferroelectric states by applying DC bias and the piezoelectric response was measured while varying the AC field amplitude. Fig. 3 presents the variation of the displacement as a function of the AC voltage amplitude for the first and second harmonics at several values of DC bias. Two regimes can be distinguished from these curves. At low excitation fields a linear increase of the displacement as a function of the AC voltage is observed in the 1st harmonic whereas a parabolic curve is obtained for the 2nd one. At high excitation fields, the displacement reaches a plateau in the 1st harmonic measurement while a fast increase is observed in the 2nd harmonic signal. For a given bias value, the onset of this second regime takes place at the same V_{AC} for both harmonics and it is correlated to the switching of the polarization. For example, the change between these two regimes is observed at $4V_{AC}$ in the case of measurements done at $3V_{DC}$ bias (indicated by arrows in Fig. 3). Accordingly, the voltage varies from -1V up to +7V during the measurement and induces the polarization switching (see fig 2 a) when approaching -1V. In conclusion, the main difference between the two vibrational regimes is the ferroelectric state of the sample: poled for low excitation fields and unpoled for the high excitation field regime. This correlation between the two harmonics indicates a common origin of both signals. The plateau in the 1st harmonic measurement can be understood as a dynamic depoling effect, like the one observed in poled ceramics when

measured in high fields [33]. In parallel, the polarization switch can be responsible for the 2nd harmonic response enhancement, as already reported for $Pb(Zr,Ti)O_3$ (PZT) films measured close to the coercive field [34].

In the following part we will focus on the low field regime. It is established by several studies, mainly realized on PZT materials, that DWs induce a nonlinear response of the 1st harmonic piezoelectric response as a function of the AC excitation [35 - 37]. This nonlinearity is not directly visible in our measurements, however it can be easily identified in fig. 4a as the deviation of calculated d_{33} from a constant value. The curves in fig. 4a show a weak linear variation of d_{33} with the AC field, linearity that depends on the DC bias used during the measurements. This linear variation can be explained using a Rayleigh model that is usually applied for subswitching conditions in hysteretic materials [38]. The Rayleigh model describes the weak field dependence of the strain by a polynomial function, which gives a linear variation of the d_{33} parameter as a function of the applied field:

$$d_{33} = d_{33}^{init} + \alpha \cdot V \qquad (2)$$

where d_{33}^{init} is the reversible Rayleigh coefficient which is related to the intrinsic response of the system plus the reversible DW displacement and α is the irreversible coefficient, associated to the irreversible motion of DWs. Accordingly, the data in fig 4a are fitted using a linear function. The d_{33}^{init} and the α values extracted from the fits are reported in fig 4b as a function of the DC bias. With increasing bias field the DW density is reduced, hence both the initial d_{33} value and the irreversible term are decreasing. Using the same Rayleigh approach, the influence of the DC bias on the nonlinearity of the dielectric coefficient was already evidenced in PZT thin films and revealed much smaller effect in the case of thinner films than for the thick ones [39]. This result was explained by the reduced DW motion in films thinner than 1µm.

The weight of the irreversible DW motion effect on the piezoelectric response can be quantified by the $\alpha \cdot V / d_{33}^{init}$ fraction. In our system, this contribution attains a maximum value of 5% for low bias values while it stays under 1% for $5V_{DC}$ bias. For comparison, 35% irreversible DW motion effects were measured on ceramic BTO materials [40]. This result sustain the idea that DW mobility is reduced in thin films.

The Rayleigh model describes correctly the piezoelectric response of the sample, however its mathematical expression allows only odd harmonics in the strain [41]. The question then arises as what is the origin of the 2nd harmonic signal measured experimentally. The aforementioned interconnection between the two harmonics sustain the idea that both signals originate from the piezoelectric activity. Recently, this assumption was demonstrated for ferroelectric materials using a modified Rayleigh model (the dynamic poling model) [41]. This theoretical approach takes into account the change in volume fraction of two adjacent 180° domains due to

the reversible motion of their separating DW driven by the alternative field. The change of volume fraction is assumed to be linear with the AC field amplitude and results in an alternative variation of the piezoelectric coefficient around its equilibrium value, expressed as:

$$d_{33}^{init}=d_0\left[1+\left(\beta+\beta'\frac{V_{AC}}{l}\right)\sin(\omega t)\right] \qquad (3)$$

with β and β' two scaling parameters and l the thickness of the film. Using a Fourier expansion of the strain, a quadratic field-dependent second harmonic term is obtained:

$$\Delta l\sim\left(\frac{\beta d_0}{2}V_{AC}+\frac{\beta' d_0}{2l}V_{AC}^2\right)\cos(2\omega t) \qquad (4)$$

were Δl represents the vertical displacement.

The dynamic poling model was successfully applied to PZT and to PYbN-PT thin films with no ferroelastic DW mobility [41, 42]. In order to verify if this theoretical approach applies to the BTO film studied here, the 2nd harmonic experimental results were fitted with a second order polynomial function and the d_0, β and β' parameters extracted from the fits were implemented in Eq. (3) to calculate the variation of d_{33}^{init} as a function of V_{AC}. The fits are represented by the lines in Fig. 5a and the polynomial parameters are presented in Fig. 5b as a function of the DC field. The data are fitted correctly, with a R^2 value larger than 0.994, except for the curve obtained for $1V_{DC}$ where the values of the displacement, close to the detection limit, coupled with a smaller number of points gives a lower $R^2 = 0.982$. Despite the good quality fits, the calculated d_{33}^{init} values are systematically larger than the measured d_{33}. This is due to the values of the quadratic coefficient $\beta' d_0/l$ that are practically twice larger than α values from fig 4b.

The model can still be enriched by taking into account the effect of electrostriction. For an AC excitation field $E_{AC}\sin(\omega t)$ the strain in the film can be written as:

$$\frac{\Delta l}{l}=M_{33}[E_{AC}\sin(\omega t)]^2=M_{33}\frac{V_{AC}^2}{l^2}\sin^2(\omega t)\Leftrightarrow\Delta l=\frac{M_{33}}{2l}V_{AC}^2[1-\cos(2\omega t)] \qquad (5)$$

with M_{33} the electrostriction coefficient. Note that the electrostriction effect should be independent of the DW density so this phenomenon could not be the origin of the observed 2nd harmonic signal. The electrostrictive displacement given by Eq. 5 was added to Eq. 4 and the experimental data were fitted with the new function. To estimate the value of the M_{33} parameter we considered that at high DC bias the electrostriction effect is predominant as the DW density is reduced. Thus, β' was considered zero for 5 V_{DC} giving $M_{33} = 7{,}6 \cdot 10^{-20} m^2/V^2$. Even if with this new fitting function the values of the $\beta' d_0/l$ parameters are decreased compared to those presented in fig. 5b, the corresponding d_{33}^{init} values are still higher than the measured d_{33} values. This

inconsistency suggests that other mechanisms may also contribute to the 2nd harmonic response of the sample. In conclusion, the dynamic poling model describes correctly the experimental data from a qualitative point of view but overestimates the effect of the reversible DW displacement on the 2nd harmonic response.

Conclusion

The piezoelectric properties of epitaxial tetragonal $BaTiO_3$ film are studied and the nonlinearities in the piezoelectric response are attributed to extrinsic effect of DW motion. The extrinsic contribution near the polarization switching field induces a large increase of the d_{33} coefficient that reaches a maximum value of 42 pm/V. In the high DC field regime, where DW contribution is reduced, the piezoelectric coefficient drops to 25 pm/V. The influence of the irreversible DW displacement on the piezoelectric response of the film was estimated by a Rayleigh approach at a maximum of 5% in the low DC field regime. The second harmonic response of the film is attributed to piezoelectric effect rather than to electrostriction, as suggested by the interconnection between the two harmonics. The 2nd harmonic measurements were qualitatively described by a modified Rayleigh model that takes into account the piezoelectric activity of the 180° DWs.

Funding

This work was funded by French Region Centre in the frame of the project COMHET.

References

1. N. Setter, D. Damjanovic, L. Eng, G. Fox, S. Gevorgian, S. Hong, A. Kingon, H. Kohlstedt, N. Y. Park, G. B. Stephenson, I. Stolitchnov, A. K. Taganstev, D. V. Taylor, T. Yamada, S. Streiffer, J. Appl. Phys., 100, 051606, (2006);
2. M. Klee, H. Boots, B. Kumar, C. van Heesch, R. Mauczok, W. Keur, M. de Wild, H. van Esch, A. L. Roest, K. Reimann, L. van Leuken, O. Wunnicke, J. Zhao, G. Schmitz, M. Mienkina, M. Mleczko, M. Tiggelman, Mat. Sci. and Eng. 8 , 012008, (2010);
3. C-B Eom, S. Trolier-McKinstry, MRS Bulletin, 37, 1007, (2012);
4. W. Liu and X. Ren, Phys. Rev. Lett. 103, 257602 (2009);
5. Z. Chen, Z. Luo, C. Huang, Y. Qi, P. Yang, L. You, C. Hu, T. Wu, J. Wang, C. Gao, T. Sritharan, L. Chen, Adv. Funct. Mater., 20, 133, (2011);

6. A. Kholkin, Ferroelectrics, 221, 219, (1999)
7. T. M. Shaw, S. Trolier-McKinstry, P.C. McIntyre, Annu. Rev. Mater. Sci., 30, 263, (2000);
8. D. Berlincourt, H. Japze, Phys. Rev., 111, 143, (1958);
9. T. Karaki, K. Yan, M. Adachi, Appl. Phys. Express 1, 111402, (2008);
10. Z. Q. Shi, Q. X. Jia, W. A. Anderson, Journal of Electronic Materials, 20, 939, (1991)
11. K. J. Choi, M. Biegalski, Y. L. Li, A. Sharan, J. Schubert, R. Uecker, P. Reiche, Y. B. Chen, X. Q. Pan, V. Gopalan, L.-Q. Chen, D. G. Schlom, C. B. Eom, Science 306, 1005 (2004);
12. A. Petraru, J. Schubert, M. Schmid, Ch. Buchal , Appl. Phys. Lett. 81, 1375, (2002);
13. W. J. Lin, T. Y. Tseng, H. B. Lu, S. L. Tu, S. J. Yang, and I. N. Lin, J. Appl. Phys., 77, 6466 (1995);
14. C. L. Li, Z. H. Chen, Y. L. Zhou, D. F. Cui, J. Phys.: Condens. Matter, 13 , 5261, (2001);
15. S.B. Mi, C.L. Jia, T. Heeg, O. Trithaveesak, J. Schubert, K. Urban, J. Crystal Growth 283 , 425; (2005);
16. J. Shin, S. V. Kalinin, A. Y. Borisevich, E. W. Plummer, A. P. Baddorf, Appl. Phys. Lett. , 91, 202901, (2007);
17. J. Hiltunen, D. Seneviratne, H. L. Tuller, J. Lappalainen, V. Lantto, J Electroceram, 22, 395, (2009);
18. D. Kan, Y. Shimakawa, Appl. Phys. Lett., 99, 081907, (2011);
19. J. F. Vignola, X. Liu, S. F. Morse, B. H. Houston, J. A. Bucaro, M. H. Marcus, D. M. Photiadis, L. Sekaric, Rev. Sci. Instr., 73, 3584, (2002)
20. R. Herdier, D. Jenkins, E. Dogheche, D. Rèmiens, M. Sulc, Rev. Sci. Instrum., 77, 093905 (2006);
21. A. Visinoiu, M. Alexe, H. N. Lee, D. N. Zakharov, A. Pignolet, D. Hesse, U. Gosele, J. Appl. Phys., 91, 10157, (2002);
22. J. Q. He, E. Vasco, R. Dittmann, R. H. Wang, Phys. Rev. B, 73, 125413 (2006);
23. D. Fu, K. Suzuki, K. Kato and H. Suzuki, Appl. Phys. A, 80, 1067 (2005);
24. C. Lichtensteiger, C. Weymann, S. Fernandez-Pena, P. Paruch and J.-M. Triscone, New J. Phys., 18, 043030, (2016);
25. M. Dawber, K. M. Rabe, J. F. Scott, Reviews Modern Physics, 77, 1083, (2005);
26. V. N. Shut, Phys. Solid State, 55, 1438, (2013);
27. H. Zheng, J. Wang, S. E. Lofland, Z. Ma, L. Mohaddes-Ardabili, T. Zhao, L. Salamanca-Riba, S. R. Shinde, S. B. Ogale, F. Bai, D. Viehland, Y. Jia, D. G. Schlom, M. Wuttig, A. Roytburd, R. Ramesh, Science, 303, 661, (2004);
28. H. Hwang, Y. Uetsuji, T. Katayama, E. Nakamachi, J. Mater. Sci, 46, 1380, (2011);

29. V. Thery, A. Bayart, J-F. Blach, P. Roussel, S. Saitzek, Appl. Surf. Sci., 351, 480, (2015);
30. P. Gao, J. Britson, J. R. Jokisaari, C. T. Nelson, S.-H. Baek, Y. Wang, C.-B. Eom, L.-Q. Chen, X. Pan, Nature Comm., 4, 2791, (2013)
31. L. Chen, A. L. Roytburd, Appl. Phys. Lett. 90, 102903, (2007);
32. N. Bassiri-Gharb, S. Trolier-McKinstry, D. Damjanovic, J. Appl. Phys., 110, 124104, (2011)].
33. A. J. Masys, W. Ren, G. Yang, B. K. Mukherjee, J. Appl. Phys. 94, 1155 (2003);
34. P. Gerber, C. Kugeler, U. Bottger, R. Waser, J. Appl. Phys., 95, 4976, (2004)
35. A. Kholkin, Ferroelectrics, 221, 219, (1999);
36. D. A. Hall, J. Mat. Sci. 36, 4575, (2001);
37. D. V. Taylor, D. Damjanovic, Appl. Phys. Lett. 76, 1615 (2000);
38. D. Damjanovic, M. Demartin, J. Phys. D: Appl. Phys. 29, 2057, (1996);
39. N. Bassiri-Gharb, I. Fujii, E. Hong, S. Trolier-McKinstry, D. V. Taylor, D. Damjanovic, J Electroceram, 19, 47, (2007);
40. D. Damjanovic, M. Demartin, J. Phys.: Condens. Matter, 9, 4943, (1997);
41. S. Trolier-McKinstry, N. Bassiri-Gharb, D. Damjanovic, Appl. Phys. Lett., 88, 202901, (2006);
42. N. Bassiri-Gharb, S.Trolier-McKinstry, D. Damjanovic, J. Appl. Phys. 100, 044107 (2006);

Figure caption:

Figure 1 a) $\theta - 2\theta$ scan showing the (001) and (002) reflections; b) reciprocal space map around the (103) Bragg reflection; c) RHEED intensity oscillations during the BTO deposition and the RHEED patterns along the STO [110] azimuth at the beginning and after 3 minutes of BTO deposition; d) AFM topography image on a 3x3 µm2 surface of BTO.

Figure 2 a) Ferroelectric hysteresis loop. b) Current density variation as a function of the DC bias; c) Piezoelectric hysteresis loop measured with 0.25V AC excitation.

Figure 3 a) 1st harmonic vertical displacement as a function of the AC excitation for several DC biases. (excitation & detection at 15 kHz); b) 2nd harmonic displacement as a function of the AC excitation for several DC biases. (excitation at 15 kHz and detection at 30 kHz).

Figure 4 a) d_{33} variation as a function of the AC excitation voltage for several DC bias. The points are experimental data and lines are linear fits; b) The fit parameters from a) as a function of the DC bias.

Figure 5 a) Vertical displacement measured at the 2nd harmonic as a function of the AC excitation for several DC bias. The points are experimental data and the lines are parabolic fits; b) Fit parameters from a) as a function of the DC bias.

Figure 1

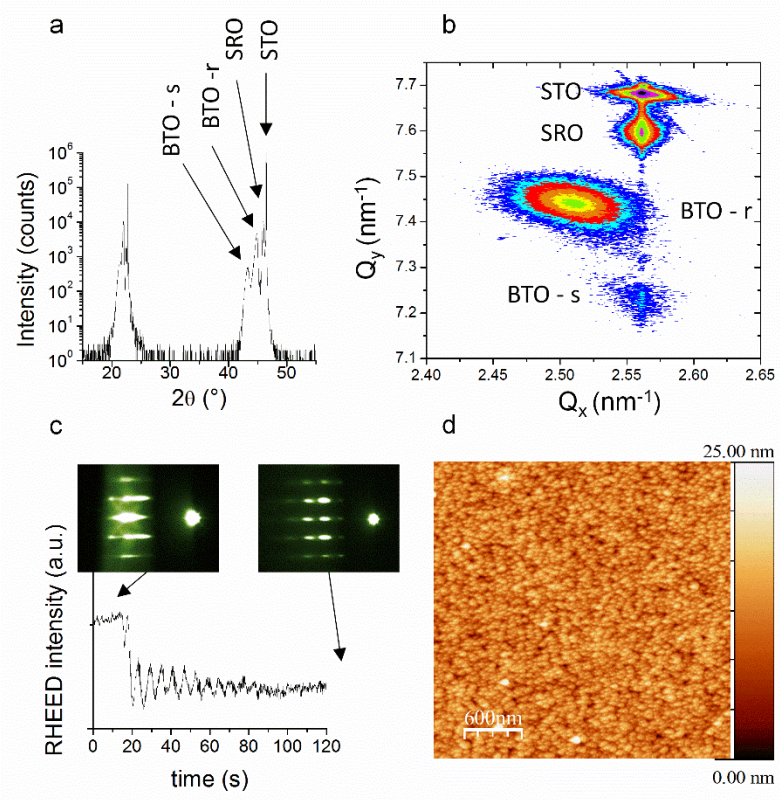
a
b
c
d
STO
SRO
BTO - r
BTO - s
Intensity (counts)
2θ (°)
Q_y (nm^{-1})
Q_x (nm^{-1})
RHEED intensity (a.u.)
time (s)
25.00 nm
0.00 nm
600nm

Figure 2

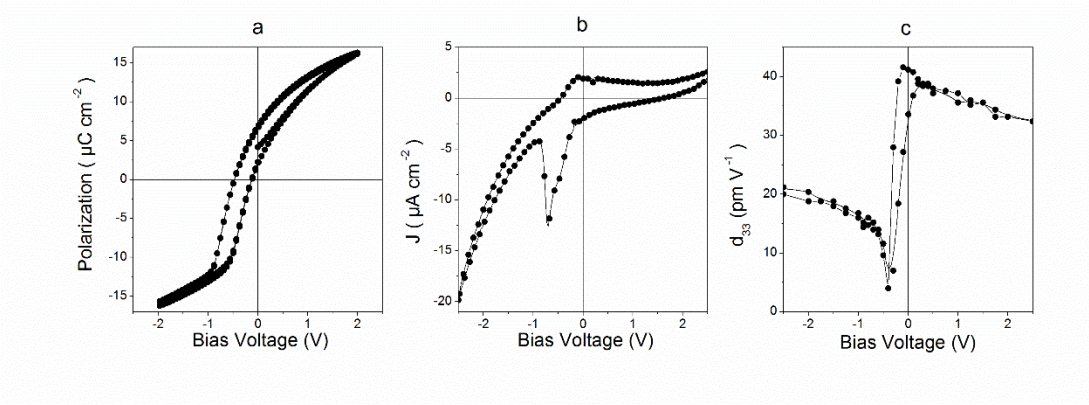
a
b
c
Polarization (μC cm -2)
J (μA cm -2)
d33 (pm V-1)
Bias Voltage (V)
Bias Voltage (V)
Bias Voltage (V)

Figure 3

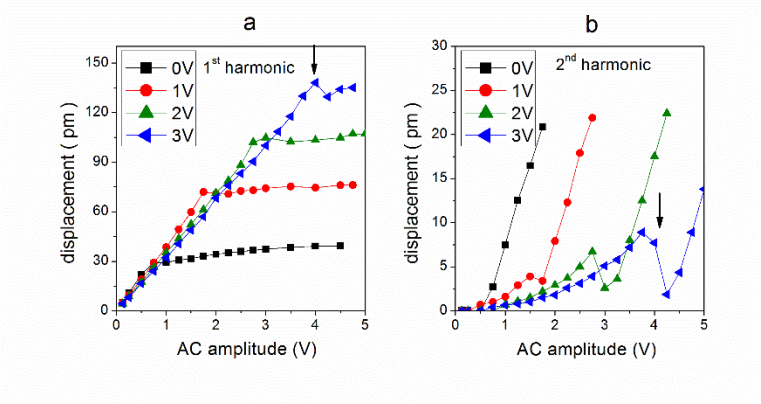
a
b
0V
1V
2V
3V
1st harmonic
2nd harmonic
displacement (pm)
AC amplitude (V)

Figure 4

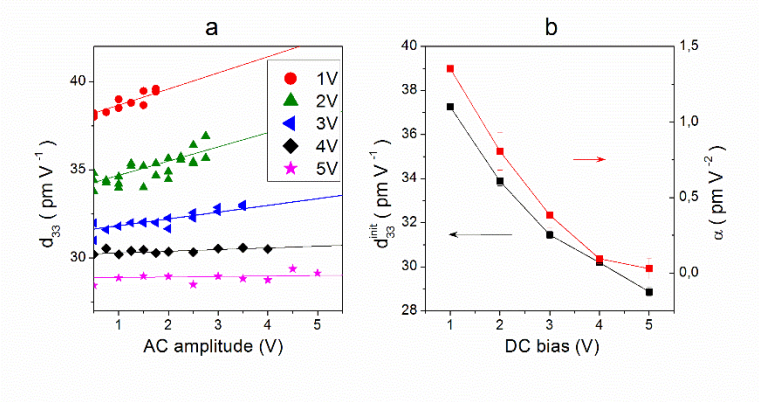
a
b
1V
2V
3V
4V
5V
d_{33} (pm V^{-1})
AC amplitude (V)
d_{33}^{init} (pm V^{-1})
α (pm V^{-2})
DC bias (V)

Figure 5

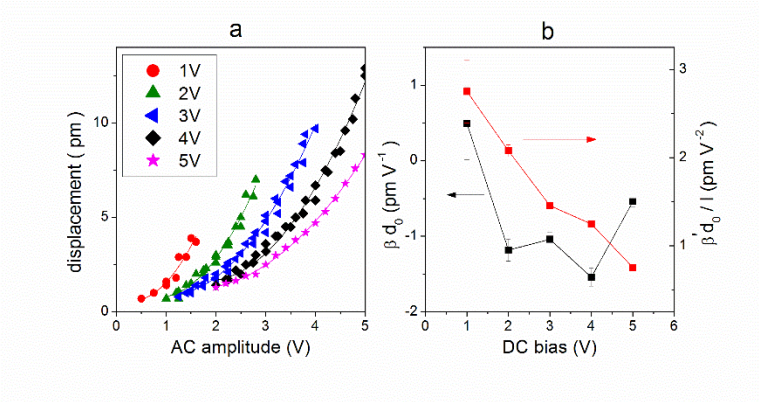
a
b
1V
2V
3V
4V
5V
displacement (pm)
AC amplitude (V)
β d0 (pm V-1)
β d0 / I (pm V-2)
DC bias (V)